Electronic Supplementary Material (ESI) for Journal of Materials Chemistry A.
This journal is © The Royal Society of Chemistry 2024

Supporting Information

Combinatorial modulation to augment all-round HER activity of Ru-CrN catalyst

Bidushi Sarkar, Barun Kumar Barman, Arko Parui, Abhishek Kumar Singh and Karuna Kar Nanda*

*Materials Research Centre, Indian Institute of Science, Bangalore-560012, India

MATERIALS AND METHODS

Chemicals

Ruthenium chloride hydrate ($RuCl_3.xH_2O$), chromium nitrate nonahydrate ($Cr(NO_3)_3 \cdot 9H_2O$), dicyandiamide (DCDA, $C_2H_4N_4$), potassium hydroxide pellets (KOH) and sulfuric acid (H_2SO_4) were purchased from Sigma Aldrich. Merck Milli-Q system is used to obtain Millipore water for the experiments.

Material synthesis

Synthesis of Ru-CrN/NCx: Ruthenium chloride (50 mg) and chromium nitrate (50 mg) were taken in a mortal – pestle to which 1 g of DCDA is added. The precursors are ground well physically to obtain a homogenous mixture. The as – obtained mixture is collected, added to a one end closed quartz tube, and kept for pyrolysis in a Lenton tube furnace at a temperature 900 °C for 1 h. The as collected sample is named Ru-CrN/NC. Similar procedure is followed to obtain Ru-CrN/NC1 and Ru-CrN/NC2 by only changing the Ru: Cr precursor amount (30:70 mg and 70:30 mg, respectively).

Synthesis of Ru/NC and Cr/NC: Control samples in the absence of Cr precursor (Ru/NC) and Ru precursor (CrN/NC) are also synthesized. 100 mg of ruthenium chloride and 1 g of DCDA is taken in a mortal – pestle, ground well and subjected to pyrolysis at 900 °C for 1 h to obtain Ru/NC. Similarly, 100 mg of chromium nitrate is taken instead of Ru precursor to obtain Cr/NC.

Material characterization

A wide-angle X-ray diffractometer (XRD, PANalytical) equipped with Cu K_α radiation, 1.54 Å is used to obtain the XRD data. A WITec system with excitation wavelength, 532 nm is used to record the Raman spectra. X-ray photoelectron spectroscopy (XPS) studies are carried out using ESCALAB 250, Thermo Scientific with monochromatic Al K_α source with 1486.6 eV. The Brunauer-Emmett-Teller (BET) surface area is studied using Autosorb iQ from Quantachrome Instruments. The energy-dispersive X-ray spectroscopy (EDX) and scanning electron microscopy (SEM) images are obtained using Karl Ziess Ultra 55 FE-SEM. FEI Titan Themis 300, accelerating voltage = 300 kV, is used to obtain high-angle annular dark-field imaging - scanning transmission electron microscopy (HAADF - STEM), transmission electron microscopy (TEM), high-resolution TEM (HRTEM) images, and elemental mapping. Inductively coupled plasma mass spectroscopy (ICP-MS) is done using a Thermo X Series II quadrupole ICPMS.

Electrochemical measurements

The electrochemical studies are performed on CH Instruments (CHI 750E) using a conventional three-electrode cell on rotating disk electrode (RDE). Graphite rod, Ag/AgCl (sat. KCl) and glassy carbon electrode (GCE, area 0.07 cm^2) are used as counter, reference

and working electrode, respectively. The HER performance of the as-synthesized catalysts is compared with commercial Pt/C (20 wt %). All the potentials measured against the reference electrode are converted and reported to potentials versus reversible hydrogen electrode (RHE). The catalyst ink is prepared by weighing 5 mg of catalyst and adding 400 μL of ethanol, 100 μL of DI water, 30 μL of 5 wt % Nafion 117 solution and sonicated for 30 minutes. 3 μL of the ink is drop casted onto GCE (catalyst loading, 0.4 mg cm^{-2}) and air-dried. The linear sweep voltammetry (LSV) is carried out at a rotation rate of 1600 rpm at scan rate of 10 mV/s and are iR-corrected (100 % compensation level). Chronoamperometry studies are done at a potential corresponding to the current density of 10 mA/cm^2. Accelerated durability tests (ADT) are done at a fast can rate (100 mV/s) for 5000 cycles. Thiocyanate poisoning test is done by adding 50 mM SCN^- in 1 M KOH solution and LSV was performed at 10 mV/s at a rotation speed of 1600.

Roughness factor (R_f) is calculated using the following equation[1],

$$R_f = ECSA/ A_g$$

Where ECSA is the electrochemically active surface area (calculated as follows)[2], and A_g is the area of the working electrode (0.07 cm^2).

$$ECSA = C_{dl}/ C_s$$

where C_{dl} is the double layer capacitance of the material and C_s is the specific capacitance, C_s = 0.040 mF/cm^2 (in alkaline) and 0.035 mF/cm^2 (in acidic media)[2].

Computational methodology

DFT calculations were done with Vienna ab initio simulation (VASP) package[3]. The Electron-ion interactions were described using all-electron projector augmented wave pseudopotentials,[4] and Perdew-Bruke-Ernzehof (PBE) generalized gradient approximation (GGA)[5] was used to approximate the electronic exchange and correlations with an on-site effective Hubbard (U_{eff} = U – J = 3 eV) parameter was used for the Cr-d states in DFT + U method as introduced by Dudarev et al.[6] The plane-wave kinetic energy cut off of 520 eV was used for bulk CrN, Ru bulk, Ru nanoparticles, unit cell of CrN (200) surface and unit cell of Ru (101) surface and 480 eV were used for all other calculations. For the heterostructure Ru/CrN, bulk CrN with optimized lattice parameters[1] a = b = c = 4.25 Å was considered to form the 4-layered (200)-oriented surface with lattice parameters, a = b = 4.25 Å and c = 26.37 Å. This was then converted to a 3×2×1 supercell with lattice parameters a = 12.75 Å, b = 8.50 Å, c = 26.37 Å. Further steps require understanding the most stable structure of Ru NPs over the CrN surface in which a nanocluster with 13 atoms was considered to have "structural magic number". The Brillouin zone was sampled using a 10×10×10, 11×11×11, 7×7×1, 4×8×1, 3×3×1, 2×4×1, 1×1×1 and 2×2×1 Monkhorst-Pack k-grid for bulk CrN, bulk Ru, unit cell of CrN (200), unit cell of Ru (101), 3×2×1 supercell of CrN (200), 3×2×1 supercell of Ru (101), isolated Ru nanoparticles and heterostructures, respectively. Bulk CrN, bulk Ru, unit cell of CrN (200), unit cell of Ru (101) and isolated Ru nanoparticles were relaxed using a conjugate gradient scheme until the energies and each component of all the forces converged to 10^{-7} eV and 0.001 eV $Å^{-1}$. For all other calculations, energy, and forces convergence to 10^{-4} eV and 0.01 eV $Å^{-1}$ were used. All the calculations are spin polarized and dipole corrected.

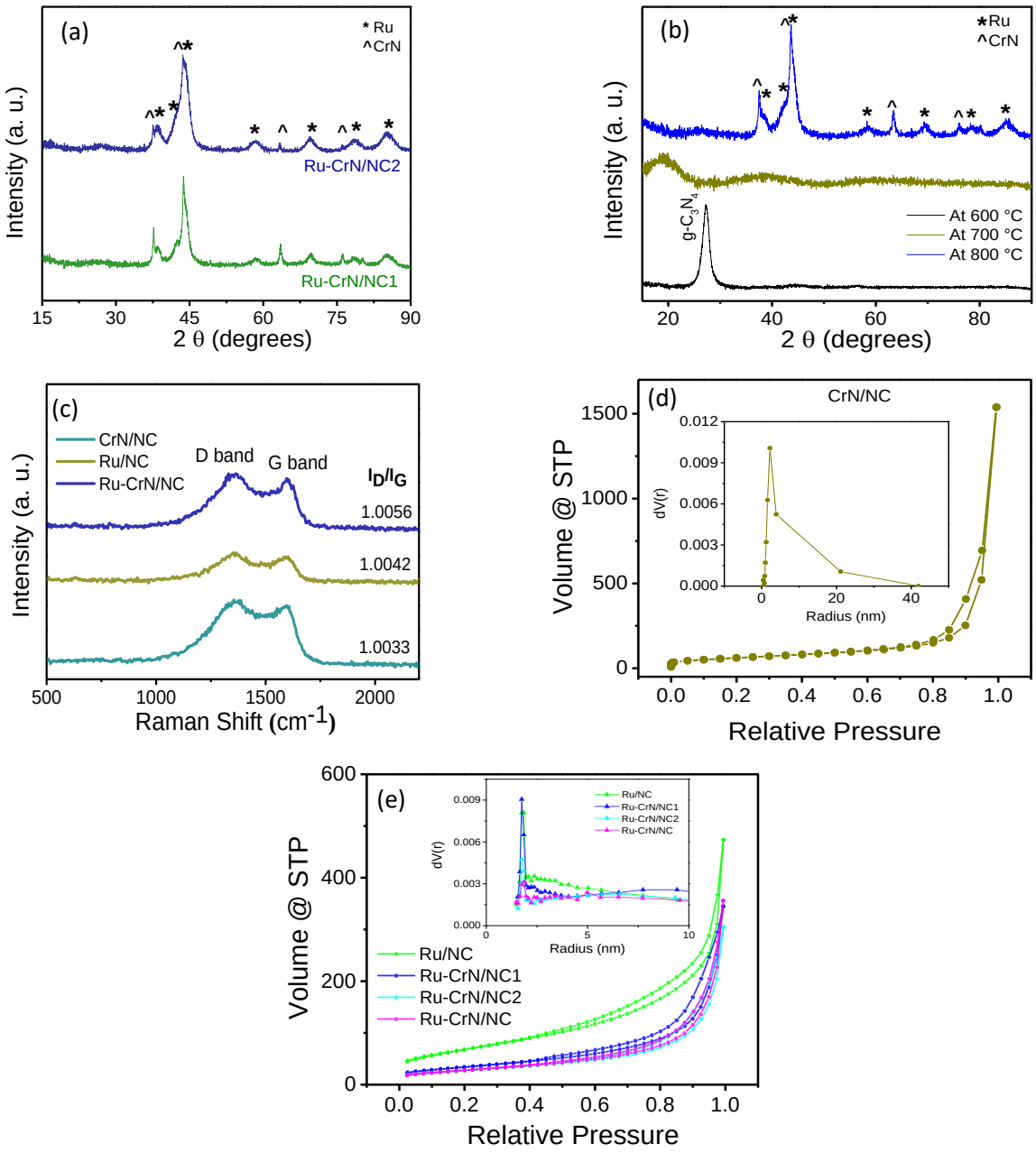

Figure S1. XRD patterns of (a) Ru-CrN/NC1 and Ru-CrN/NC2, (b) the intermediate at 600 to 800 °C during the synthesis of Ru-CrN/NC, (c) Raman spectra of the samples, (d) Nitrogen adsorption – desorption isotherm of CrN/NC, inset: pore size distribution curve, (e) Nitrogen adsorption – desorption isotherm of different samples, inset: pore size distribution curve of the samples.

Table S1. Surface area, pore radius and volume as obtained by as obtained by BET and BJH method, respectively.

	Surface area (m^2/g)	Pore radius (nm)	Pore volume (cc/g)
CrN/NC	217.02	2.19	2.38
Ru/NC	246.70	1.75	0.69
Ru-CrN/NC1	114.31	1.75	0.53
Ru-CrN/NC2	99.64	1.75	0.47
Ru-CrN/NC	108.84	1.78	0.54

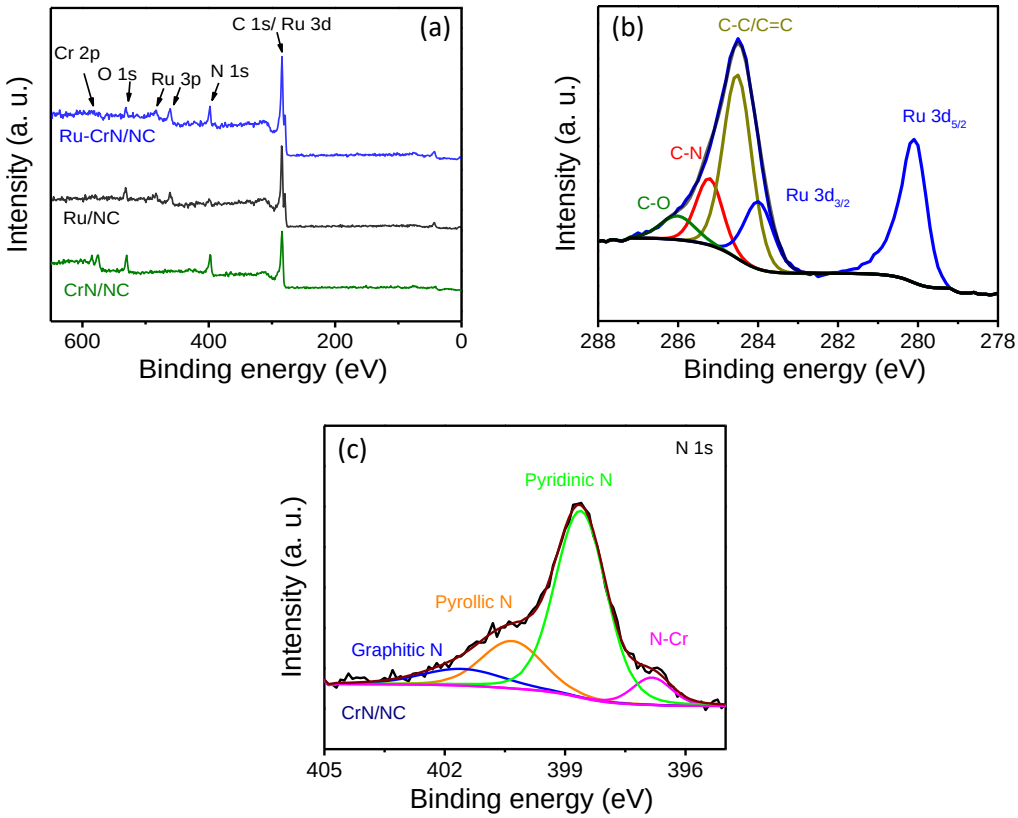

Figure S2. (a) XPS survey spectra of the samples, and (b) C 1s of Ru-CrN/NC and (c) HRXPS N 1s spectra of CrN/NC.

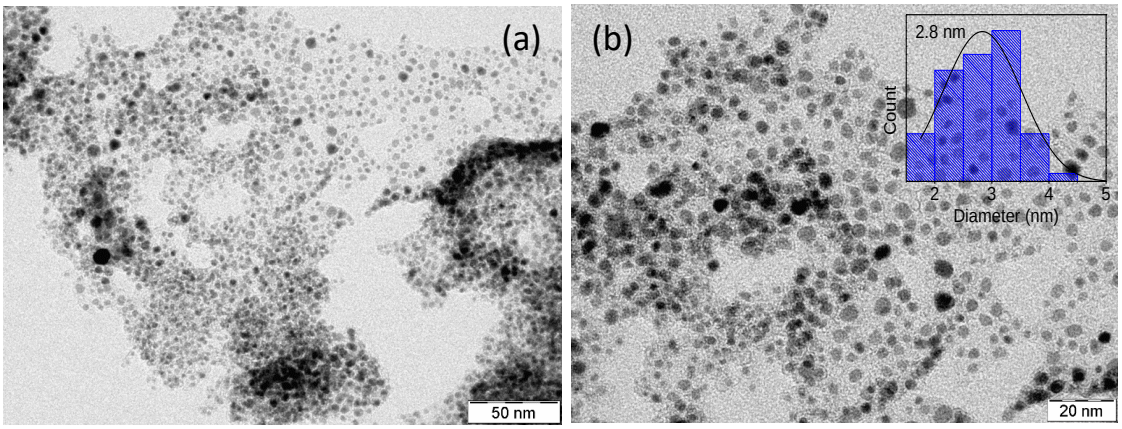

Figure S3. (a, b) TEM images of Ru/NC, inset; size distribution curve.

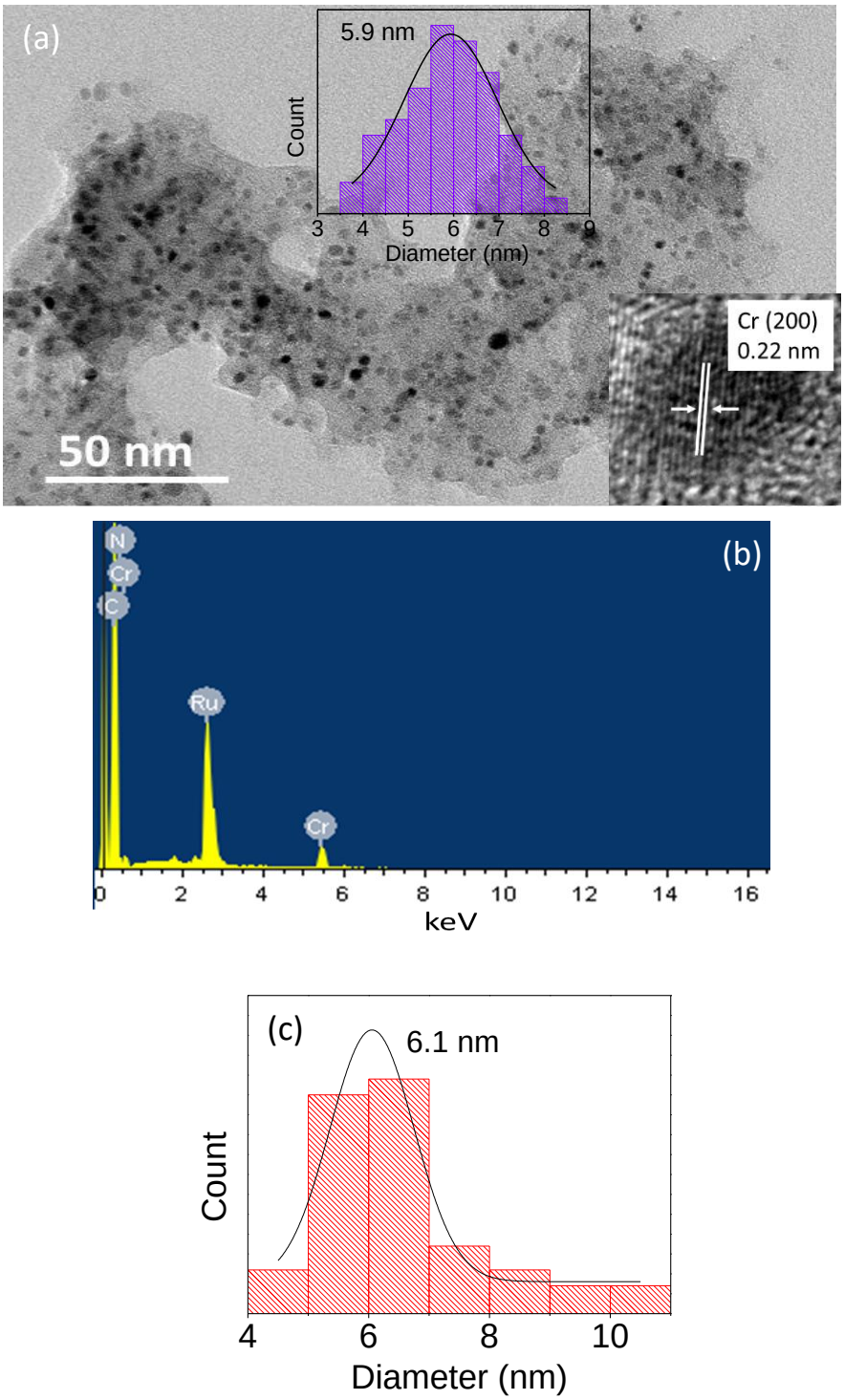

Figure S4. (a) TEM, inset: HRTEM and size distribution curve of CrN/NC. and (b) EDS spectrum of Ru-CrN/NC, (c) particle size distribution curve for Ru-CrN/NC.

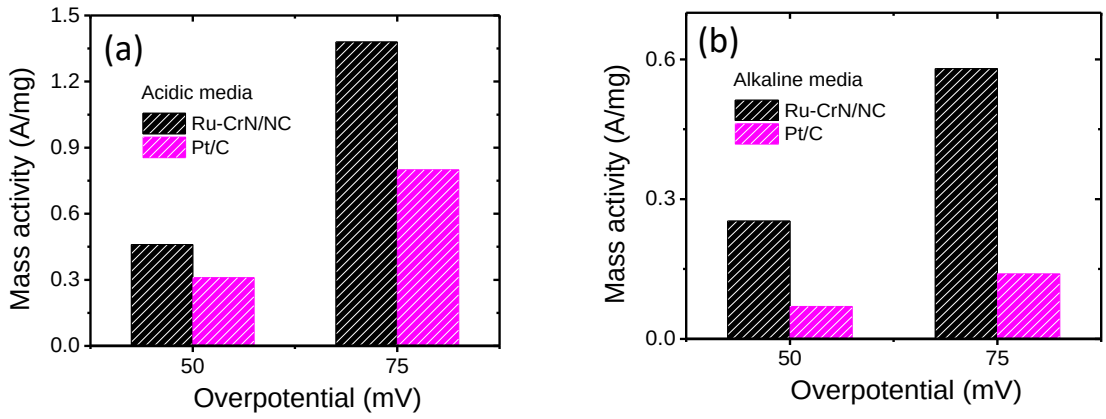

Figure S5. Mass activity of Ru-CrN/NC and Pt/C in (a) acidic, and (b) alkaline media.

Table S2. Comparison of the HER activity with previously reported Ru hybrid catalysts in alkaline media.

Catalyst	**Loading (mg/cm^2)**	**Medium**	**E@10 mA/cm^2 (mV)**	**Tafel slope (mV/dec)**	**Reference**
Ru-CrN/NC	***0.4***	***1 M KOH***	***53***	***59***	***This work***
$Ru/C_3N_4/C$	0.204	1 M KOH	79	-	[7]
RuP_2@NPC	1.00	1 M KOH	52	69	[8]
RuO_2/Co_3O_4	-	1 M KOH	89	91	[9]
Ultrafine Ru/NG tube	0.428	1 M KOH	45	81	[10]
Ru@NGT	0.428	1 M KOH	60	81	[11]
1D-RuO_2-CN	0.17	0.5 M KOH	95	70	[12]
Cu_{2-x}@RuNPS	0.23	1 M KOH	82	48	[13]
$Ru@RuO_2$	-	0.1 M KOH	137	113	[14]
Ultrafine Ru/N graphene	-	1 M KOH	40	76	[15]
RuO_2/Ni foam	-	1 M KOH	60	-	[16]

Table S3. Comparison of the HER activity with previously reported Ru hybrid catalysts in acidic media.

Catalyst	**Loading (mg/cm^2)**	**Medium**	**E@10 mA/cm^2 (mV)**	**Tafel slope (mV/dec)**	**Reference**
Ru-CrN/NC	***0.4***	**0.5 M H_2SO_4**	***41***	***37***	***This work***
Ru@C_2N	0.285	0.5 M H_2SO_4	135	30	[17]
Cu_{2-x}@RuNPS	0.23	0.5 M H_2SO_4	129	51	[13]
$Ni_{43}Ru_{57}$ nanoalloy	0.28	0.5 M H_2SO_4	41	31	[18]
Ultrafine Ru/N graphene	-	1 M H_2SO_4	60	41	[15]
Ru@MoO_2	0.285	0.5 M H_2SO_4	55	44	[19]
C_3N_4-Ru-F	0.153	0.5 M H_2SO_4	140	57	[20]
Ru/NG-750	-	0.5 M H_2SO_4	53	44	[21]
Ru@CN-0.16	-	0.5 M H_2SO_4	126	-	[22]

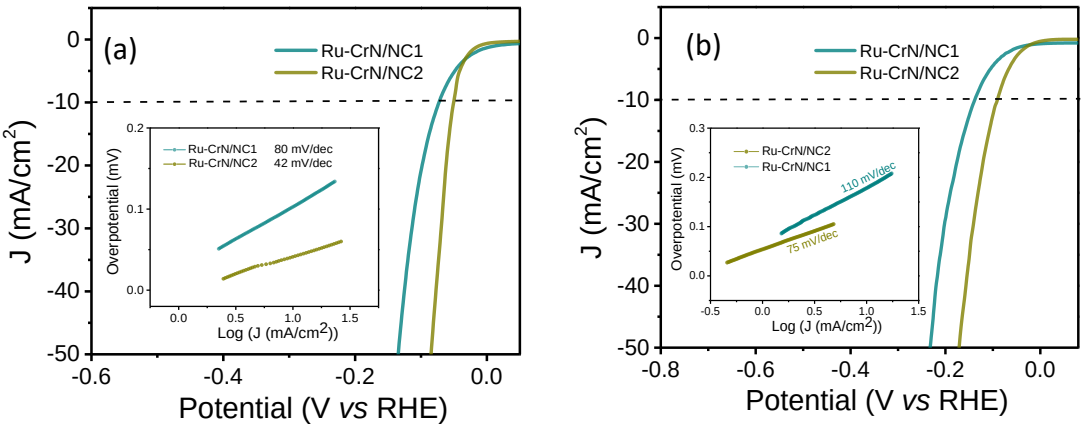

Figure S6. LSV polarization of Ru-CrN/NC1 and Ru-CrN/NC2, inset, corresponding Tafel slope in (a) 1 M KOH, and (b) 0.5 M H_2SO_4.

Table S4. Content of Ru and Cr (weight %) in the respective samples as obtained by ICP-MS measurements.

	Ru %	*Cr %*
Ru-CrN/NC	8.7	2.9
Ru-CrN/NC1	6.3	3.7
Ru-CrN/NC2	11.4	1.5

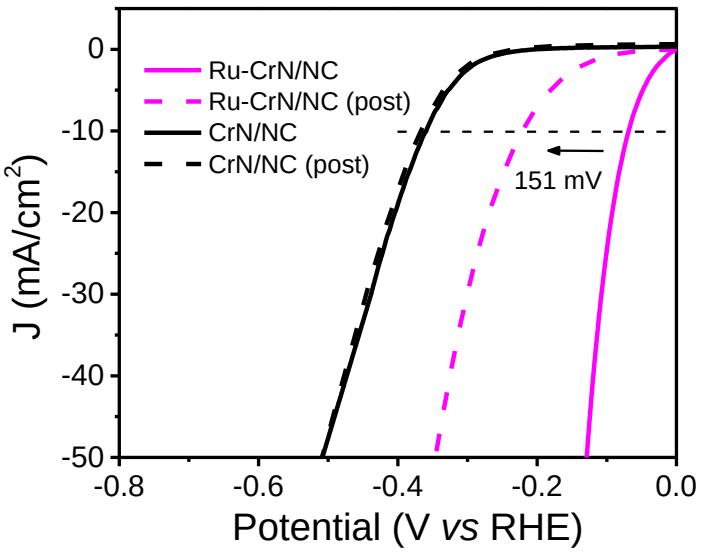

Figure S7. LSV curve of Ru-CrN/NC and CrN/NC before and post adding 50 mM KSCN in 1 M KOH.

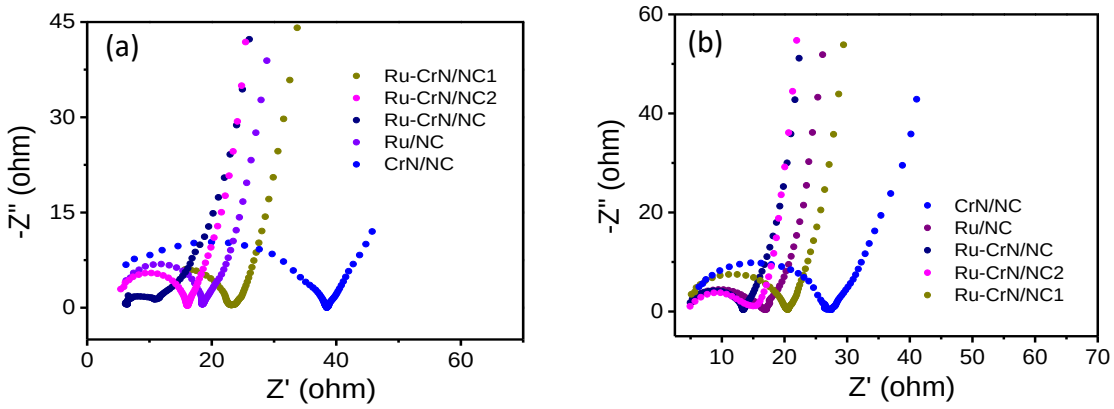

Figure S8. Nyquist plots in (a) 1 M KOH, and (b) 0.5 M H_2SO_4.

Table S5. Charge transfer and solution resistance (R_{CT} + R_s) as obtained from Nyquist plots.

	R_{CT} + R_S (Ω)	
	Alkaline media	**Acidic media**
Ru/NC	18.51	16.89
CrN/NC	38.42	27.30
Ru-CrN/NC1	23.33	20.46
Ru-CrN/NC2	16.02	15.53
Ru-CrN/NC	11.09	13.19

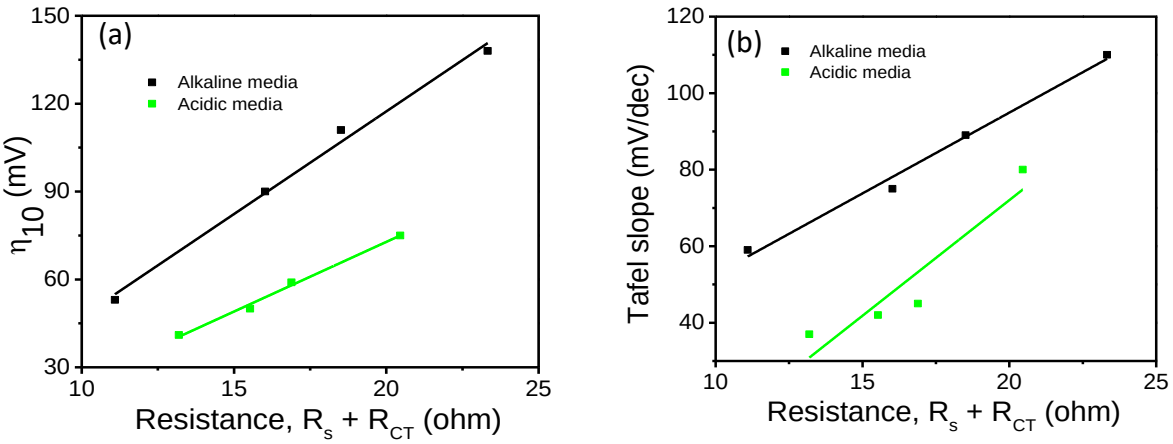

Figure S9. Relationship between (a) η_{10} and (b) Tafel slope with resistance (Rs + R_{CT}) in alkaline and acidic media for as-synthesized Ru/NC, Ru-CrN/NC, Ru-CrN/NC1 and Ru-CrN/NC2.

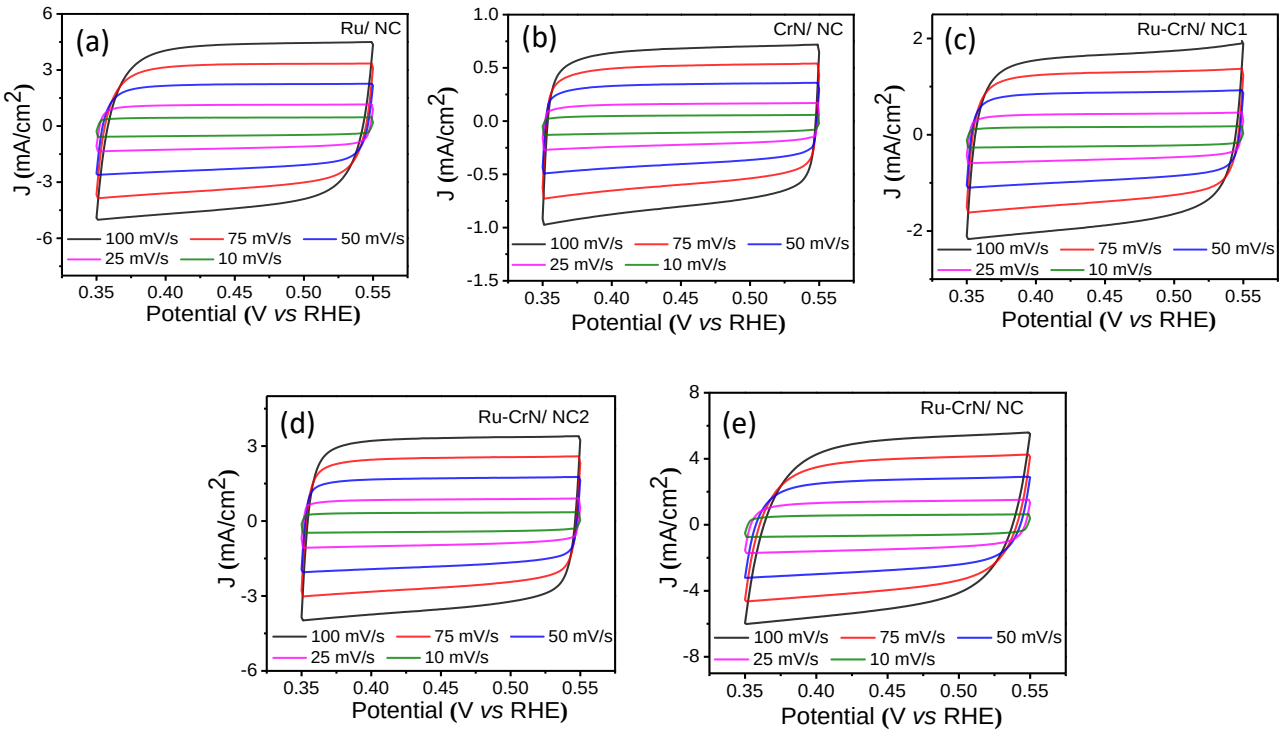

Figure S10. Cyclic voltammetry (CV) in the non – faradaic region at different scan rates (10 to 100 mV/s) for (a) Ru/NC, (b) CrN/NC, (c) Ru-CrN/NC1, (d) Ru-CrN/NC2, (e) Ru-CrN/NC in 1 M KOH.

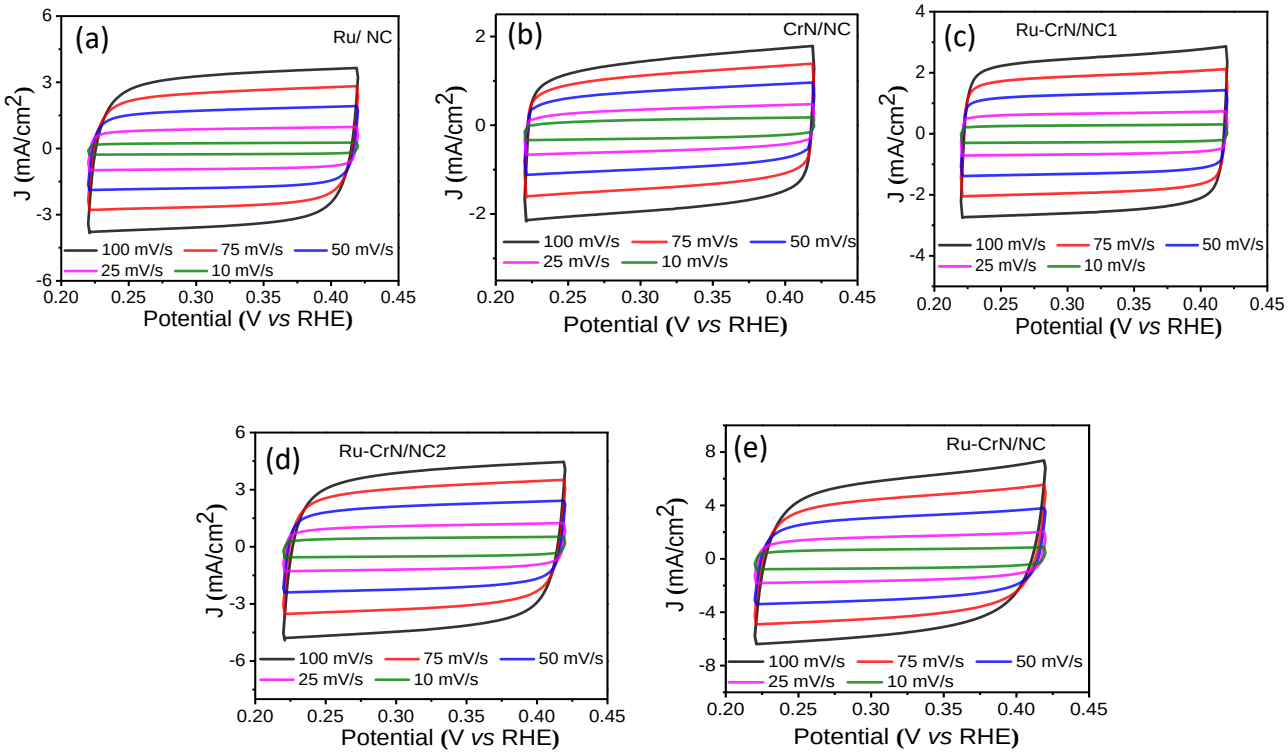

Figure S11. Cyclic voltammetry (CV) in the non – faradaic region at different scan rates (10 to 100 mV/s) for (a) Ru/NC, (b) CrN/NC, (c) Ru-CrN/NC1, (d) Ru-CrN/NC2, (e) Ru-CrN/NC in 0.5 M H_2SO_4.

Table S6. Electroactive surface area (ECSA) and roughness factor (R_f) for different samples.

	Alkaline media		Acidic media	
	ECSA (cm^2)	R_f	ECSA (cm^2)	R_f
Ru-CrN/NC	84	1200	96	1371.42857
Ru-CrN/NC1	70	1000	80	1142.85714
Ru-CrN/NC2	26.25	375	30	428.57143
Ru/NC	54.25	775	62	885.71429
CrN/NC	12.25	175	14	200

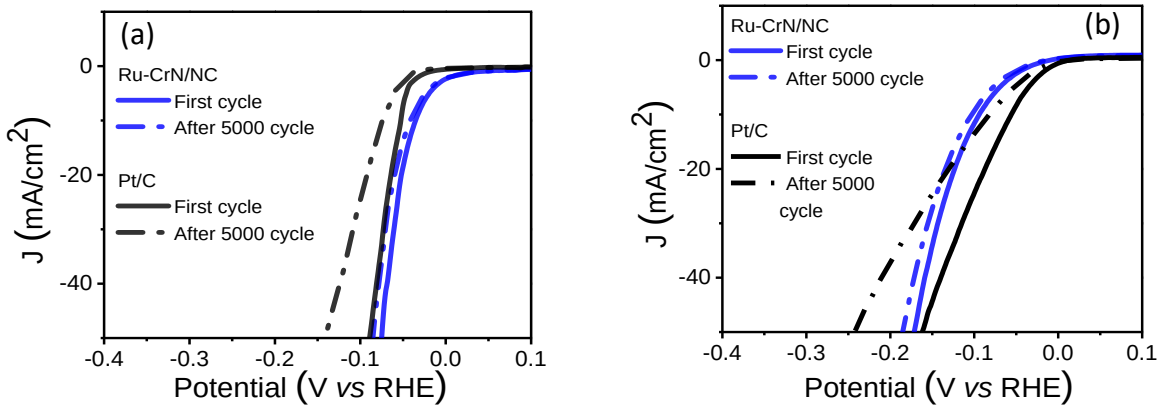

Figure S12. ADT done at a scan rate of 100 mV/s in a potential range of 0.1 to -0.4 V at rotation speed of 1600 rpm for Ru-CrN/NC and Pt/C in (a) 1 M KOH, and (b) 0.5 M H_2SO_4.

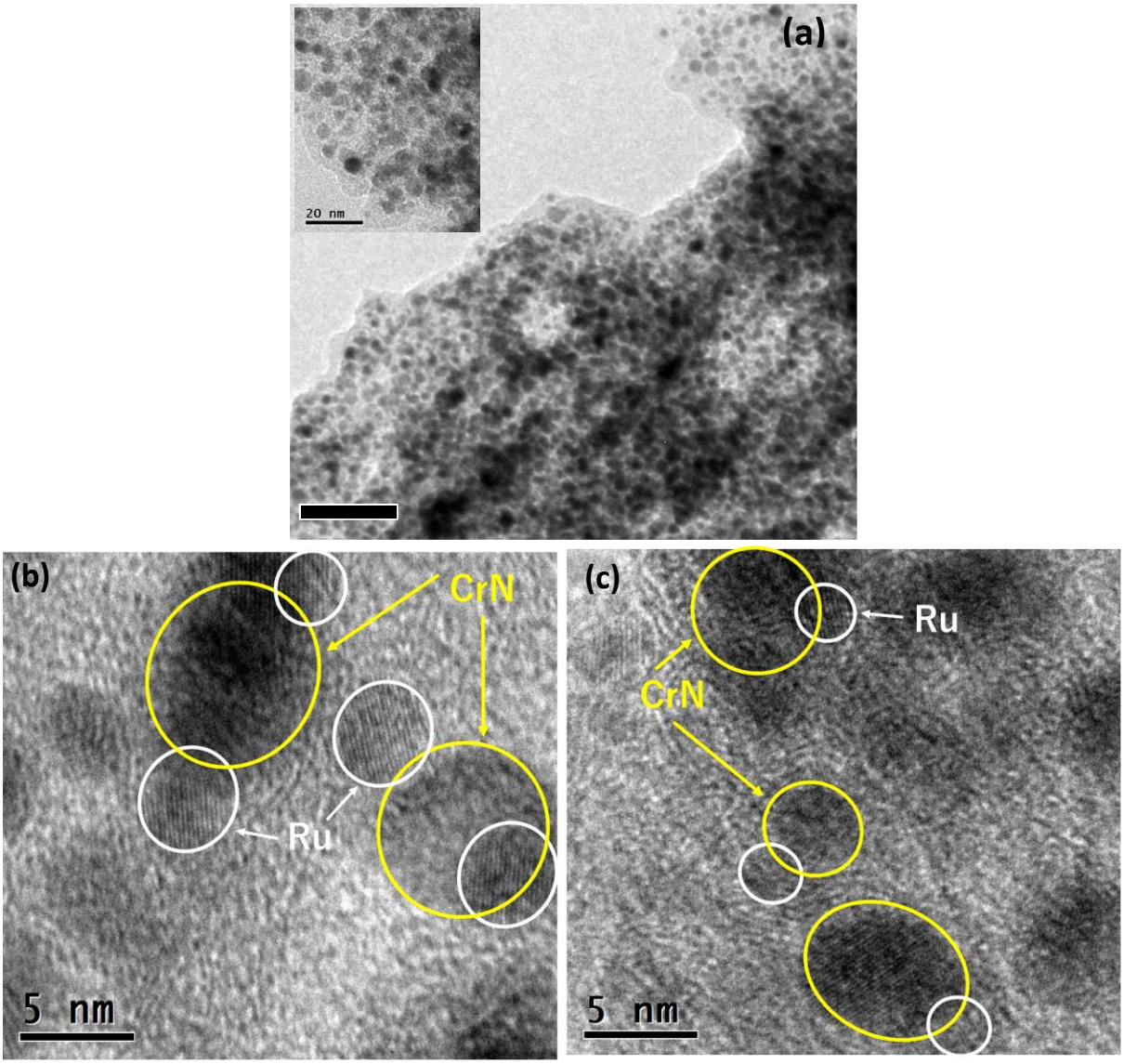

Figure S13. (a, b) TEM and HRTEM image of Ru-CrN/NC after stability tests in alkaline media and (c) in acidic media depicting the retained heterointerface (Ru-CrN). Scale bar (a) 50 nm, (b and c) 5 nm

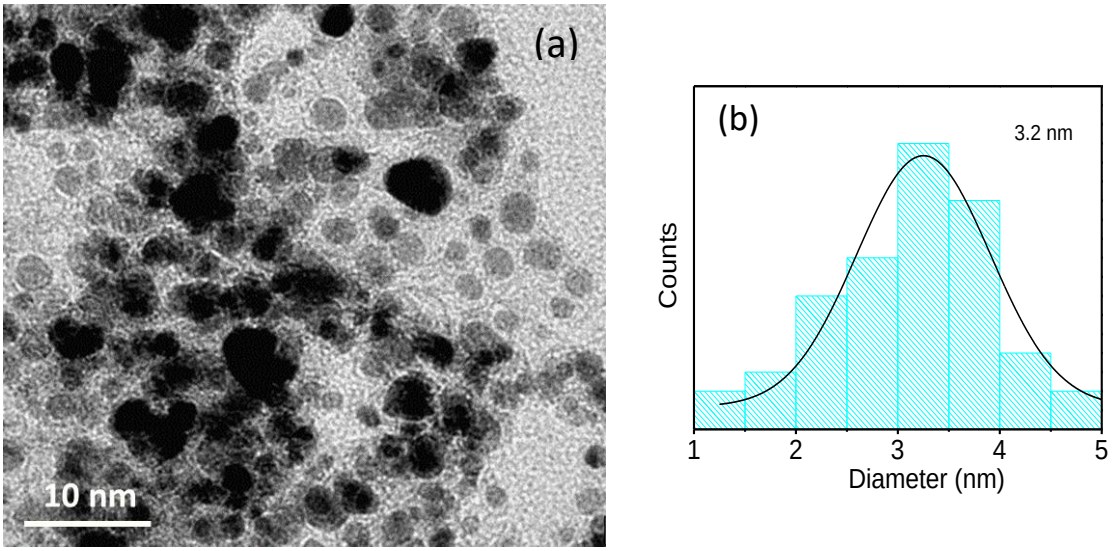

Figure S14. (a)TEM image and (b) size distribution curve of Ru/NC post HER in alkaline media.

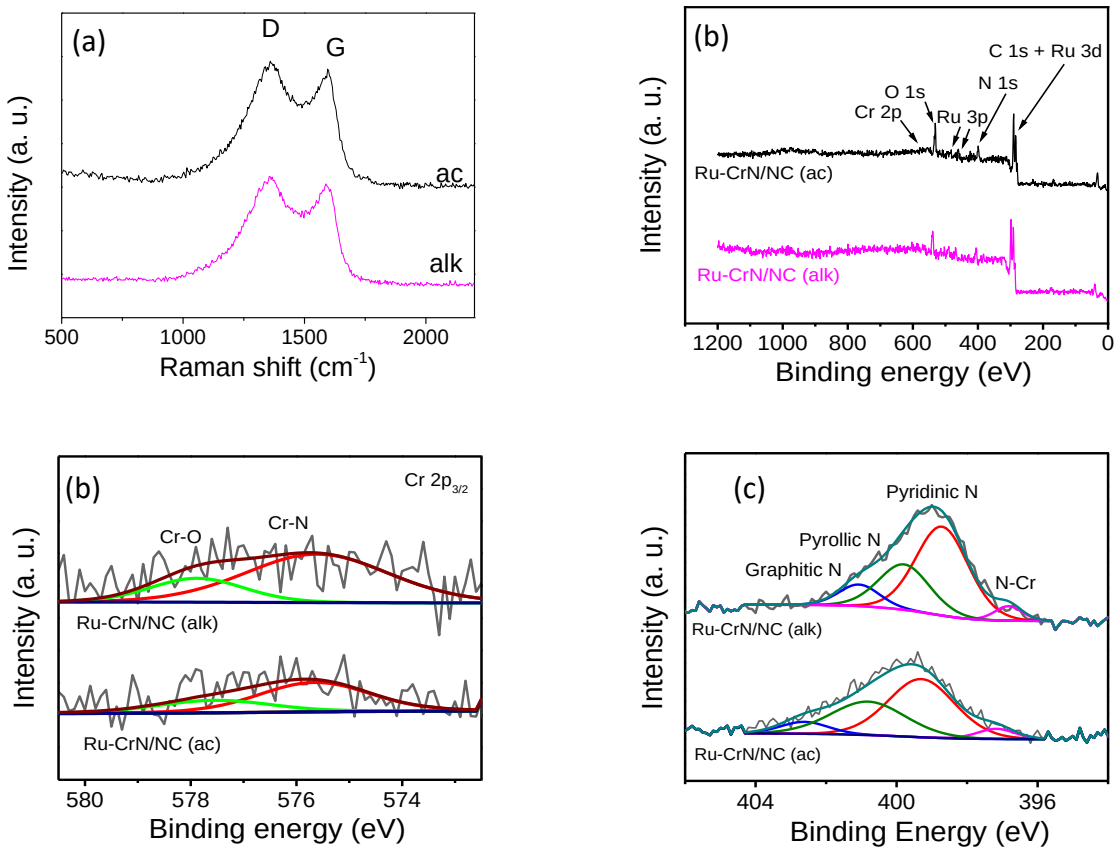

Figure S15. (a) Raman spectra, (b) XPS survey spectra, HRXPS of (b) Cr 2p, and (c) N 1s after the long-term stability test in acidic and alkaline media for Ru-CrN/NC.

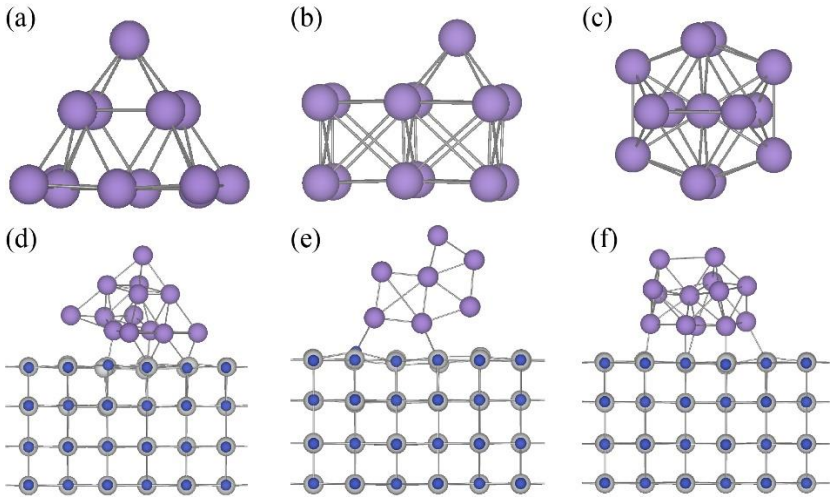

Figure S16. (a) Ru (1), (b) Ru (2), and (c) Ru (3) are the different considered isolated Ru nanoparticles and (d) Ru-CrN (1), (e) Ru-CrN (2) and (f) Ru-CrN (3) are the correspondingly optimized Ru-CrN heterostructures, respectively. Grey, Blue and purple balls represent the Cr, N and Ru atoms, respectively.

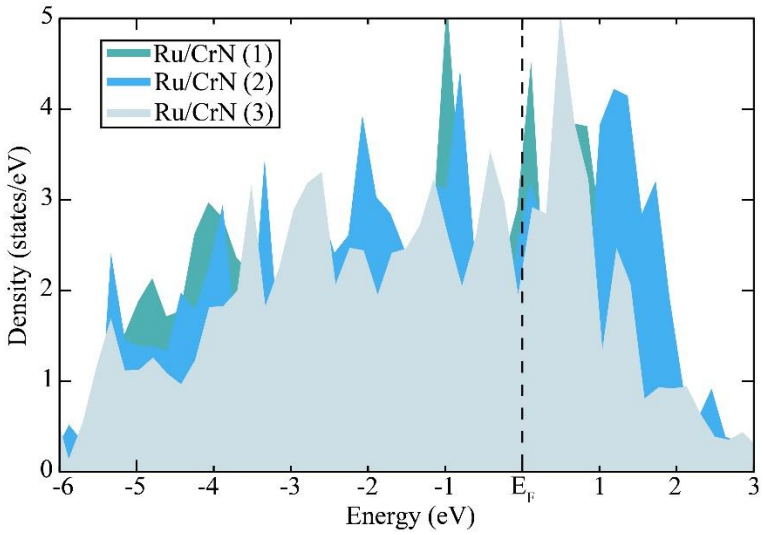

Figure S17. Total density of states for d-band of different Ru nanoparticles supported over CrN.

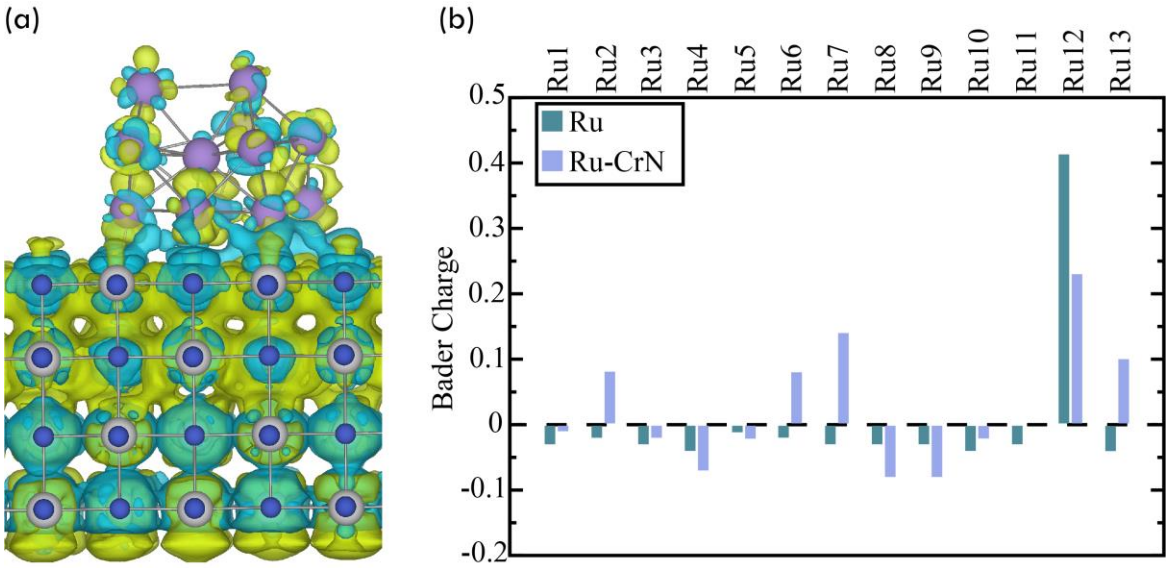

Figure S18. (a) Charge separation diagram of Ru-CrN where the yellow and blue regions show the electron depleted and accumulated regions. (b) Comparison of Bader charge of Ru atoms in between isolated Ru nanoparticles and Ru supported over CrN (Ru-CrN).

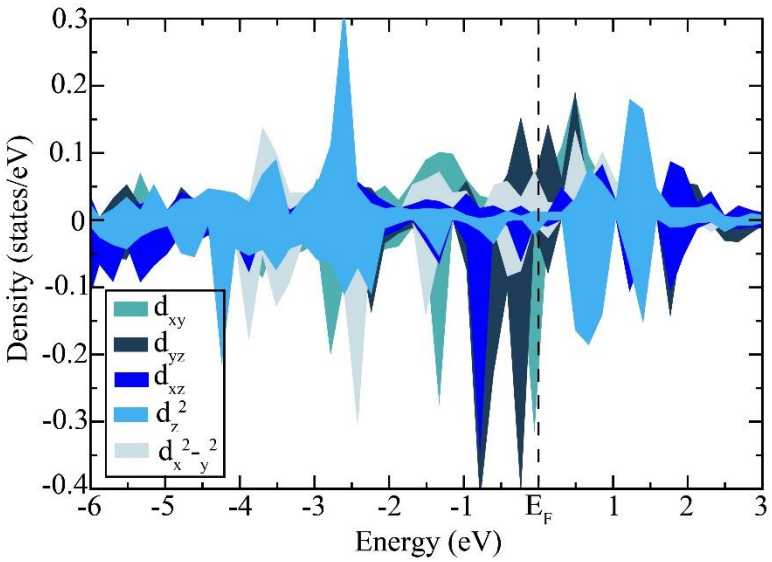

Figure S19. Partial density of states for d-band of Ru atom of Ru-CrN.

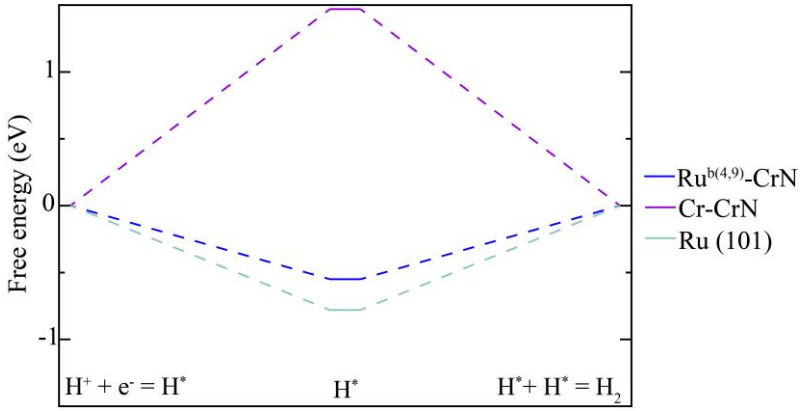

Figure S20. Free energy diagram for HER over bridge site of Ru4 and Ru9, on top position of Cr of Ru-CrN and (101)-oriented surface of Ru.

Free energy diagram for HER for the differently considered active sites over Ru nanoparticles of Ru-CrN where the 'b' describes bridge positions between the atoms given inside the brackets whereas rest describes the on top position.

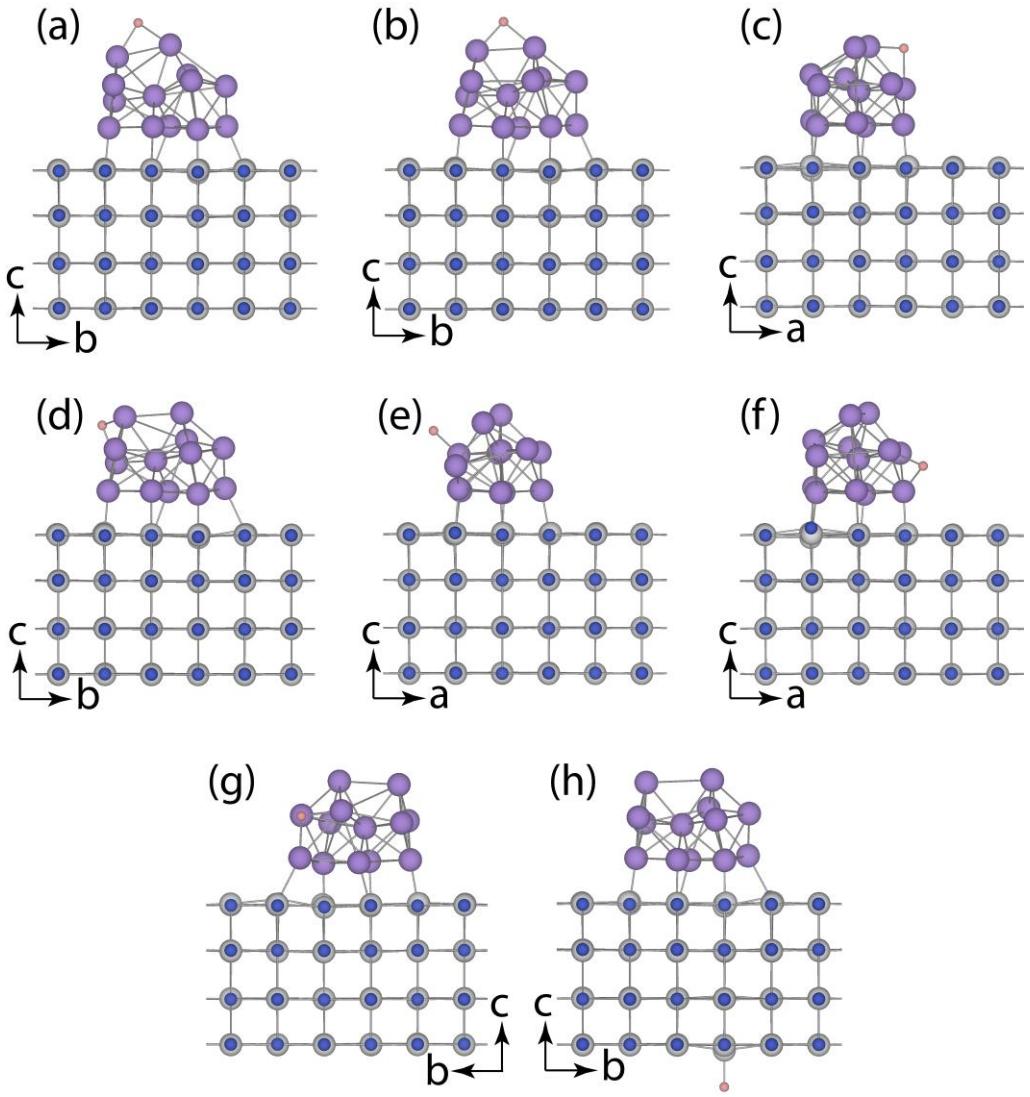

Figure S21. Optimized structures of adsorbed H* intermediate over different adsorption sites of Ru-CrN.

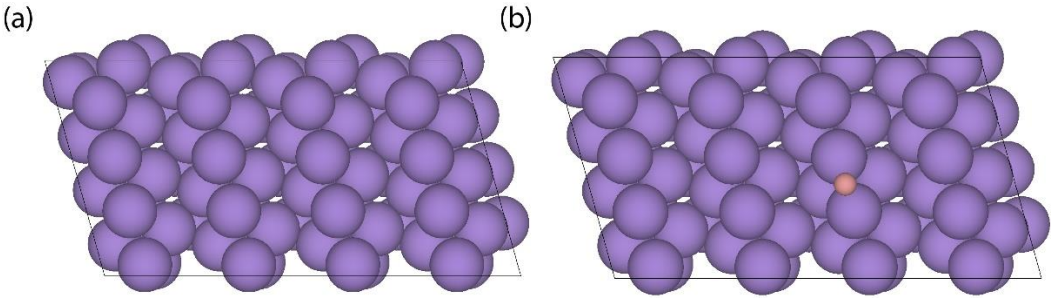

Figure S22. (a) Top view of Ru (101) surface. (b) Top view of adsorbed H* intermediate over the Ru (101) surface.

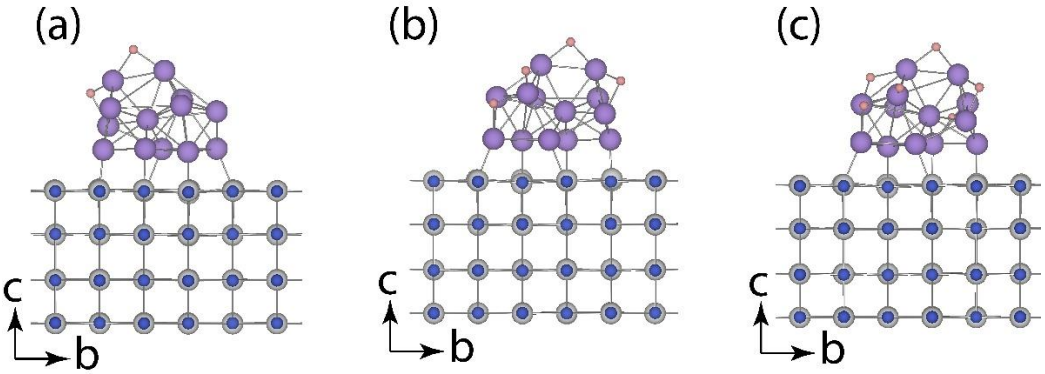

Figure S23. Optimized structure of H* intermediates where the coverages are (a) 33.33 %, (b) 66.66 % and (c) 100 %.

Table S7: Adsorption energy, free energy corrections and free energy for H* adsorption on different active sites.

Atom	Adsorption energy (eV)	ΔZPE-TΔS	Free energy (eV)	Average d-band center (up)	Average d-band center (down)
$Ru^{b(4,8)}$-CrN	-1.04	0.02	-1.06	-1.45	-1.24
$Ru^{b(4,8)}$-CrN	-0.75	0.02	-0.77	-1.45	-1.24
$Ru^{b(8,10)}$-CrN	-0.65	0.02	-0.67	-1.43	-1.41
$Ru^{b(4,9)}$-CrN	-0.53	0.02	-0.55	-1.48	-1.16
Ru^{1}-CrN	-0.83	0.02	-0.85	-1.58	-1.20
$Ru^{b(8,11)}$-CrN	-0.7	0.02	-0.72	-1.56	-1.40
Ru^{6}-CrN	-0.59	0.02	-0.61	-1.18	-1.60
Cr-CrN	1.45	0.02	1.47		
Ru (101)	-0.76	0.02	-0.78		

Table S8. Coverage-dependent average adsorption energy of H* intermediate for Ru-CrN system

Surface coverage	Adsorption energy (eV)
33.33 %	-0.82
66.66 %	-0.66
100 %	-0.63

References

1. Nandan, R.; Gautam, A.; Tripathi, S.; Nanda, K. K., A comprehensive analysis and rational designing of efficient Fe-based oxygen electrocatalysts for metal–air batteries. *Journal of Materials Chemistry A* **2018,** *6* (18), 8537-8548.
2. McCrory, C. C. L.; Jung, S.; Peters, J. C.; Jaramillo, T. F., Benchmarking Heterogeneous Electrocatalysts for the Oxygen Evolution Reaction. *Journal of the American Chemical Society* **2013,** *135* (45), 16977-16987.
3. Kresse, G.; Hafner, J., Ab initio molecular dynamics for liquid metals. *Physical Review B* **1993,** *47* (1), 558-561.

4. Kresse, G.; Joubert, D., From ultrasoft pseudopotentials to the projector augmented-wave method. *Physical Review B* **1999,** *59* (3), 1758-1775.
5. Perdew, J. P.; Burke, K.; Ernzerhof, M., Generalized Gradient Approximation Made Simple. *Physical Review Letters* **1996,** *77* (18), 3865-3868.
6. Dudarev, S. L.; Botton, G. A.; Savrasov, S. Y.; Humphreys, C. J.; Sutton, A. P., Electron-energy-loss spectra and the structural stability of nickel oxide: An LSDA+U study. *Physical Review B* **1998,** *57* (3), 1505-1509.
7. Zheng, Y.; Jiao, Y.; Zhu, Y.; Li, L. H.; Han, Y.; Chen, Y.; Jaroniec, M.; Qiao, S.-Z., High Electrocatalytic Hydrogen Evolution Activity of an Anomalous Ruthenium Catalyst. *Journal of the American Chemical Society* **2016,** *138* (49), 16174-16181.
8. Pu, Z.; Amiinu, I. S.; Kou, Z.; Li, W.; Mu, S., RuP2-Based Catalysts with Platinum-like Activity and Higher Durability for the Hydrogen Evolution Reaction at All pH Values. *Angewandte Chemie International Edition* **2017,** *56* (38), 11559-11564.
9. Liu, H.; Xia, G.; Zhang, R.; Jiang, P.; Chen, J.; Chen, Q., MOF-derived RuO2/Co3O4 heterojunctions as highly efficient bifunctional electrocatalysts for HER and OER in alkaline solutions. *RSC Advances* **2017,** *7* (7), 3686-3694.
10. Barman, B. K.; Sarkar, B.; Nanda, K. K., Pd-coated Ru nanocrystals supported on N-doped graphene as HER and ORR electrocatalysts. *Chemical Communications* **2019,** *55* (92), 13928-13931.
11. Barman, B. K.; Sarkar, B.; Ghosh, P.; Ghosh, M.; Mohan Rao, G.; Nanda, K. K., In Situ Decoration of Ultrafine Ru Nanocrystals on N-Doped Graphene Tube and Their Applications as Oxygen Reduction and Hydrogen Evolution Catalyst. *ACS Applied Energy Materials* **2019,** *2* (10), 7330-7339.
12. Bhowmik, T.; Kundu, M. K.; Barman, S., Growth of One-Dimensional RuO2 Nanowires on g-Carbon Nitride: An Active and Stable Bifunctional Electrocatalyst for Hydrogen and Oxygen Evolution Reactions at All pH Values. *ACS Applied Materials & Interfaces* **2016,** *8* (42), 28678-28688.
13. Yoon, D.; Lee, J.; Seo, B.; Kim, B.; Baik, H.; Joo, S. H.; Lee, K., Cactus-Like Hollow Cu2-xS@Ru Nanoplates as Excellent and Robust Electrocatalysts for the Alkaline Hydrogen Evolution Reaction. *Small* **2017,** *13* (29), 1700052.
14. Jiang, R.; Tran, D. T.; Li, J.; Chu, D., Ru@RuO2 Core-Shell Nanorods: A Highly Active and Stable Bifunctional Catalyst for Oxygen Evolution and Hydrogen Evolution Reactions. *ENERGY & ENVIRONMENTAL MATERIALS* **2019,** *2* (3), 201-208.
15. Barman, B. K.; Das, D.; Nanda, K. K., Facile synthesis of ultrafine Ru nanocrystal supported N-doped graphene as an exceptional hydrogen evolution electrocatalyst in both alkaline and acidic media. *Sustainable Energy & Fuels* **2017,** *1* (5), 1028-1033.
16. Lee, J.; Sher Shah, S. A.; Yoo, P. J.; Lim, B., Hydrous RuO2 nanoparticles as highly active electrocatalysts for hydrogen evolution reaction. *Chemical Physics Letters* **2017,** *673*, 89-92.
17. Mahmood, J.; Li, F.; Jung, S.-M.; Okyay, M. S.; Ahmad, I.; Kim, S.-J.; Park, N.; Jeong, H. Y.; Baek, J.-B., An efficient and pH-universal ruthenium-based catalyst for the hydrogen evolution reaction. *Nature Nanotechnology* **2017,** *12* (5), 441-446.
18. Zhang, C.; Liu, Y.; Chang, Y.; Lu, Y.; Zhao, S.; Xu, D.; Dai, Z.; Han, M.; Bao, J., Component-Controlled Synthesis of Necklace-Like Hollow NiXRuy Nanoalloys as Electrocatalysts for Hydrogen Evolution Reaction. *ACS Applied Materials & Interfaces* **2017,** *9* (20), 17326-17336.
19. Jiang, P.; Yang, Y.; Shi, R.; Xia, G.; Chen, J.; Su, J.; Chen, Q., Pt-like electrocatalytic behavior of Ru–MoO2 nanocomposites for the hydrogen evolution reaction. *Journal of Materials Chemistry A* **2017,** *5* (11), 5475-5485.
20. Peng, Y.; Lu, B.; Chen, L.; Wang, N.; Lu, J. E.; Ping, Y.; Chen, S., Hydrogen evolution reaction catalyzed by ruthenium ion-complexed graphitic carbon nitride nanosheets. *Journal of Materials Chemistry A* **2017,** *5* (34), 18261-18269.
21. Ye, R.; Liu, Y.; Peng, Z.; Wang, T.; Jalilov, A. S.; Yakobson, B. I.; Wei, S.-H.; Tour, J. M., High Performance Electrocatalytic Reaction of Hydrogen and Oxygen on Ruthenium Nanoclusters. *ACS Applied Materials & Interfaces* **2017,** *9* (4), 3785-3791.

22. Wang, J.; Wei, Z.; Mao, S.; Li, H.; Wang, Y., Highly uniform Ru nanoparticles over N-doped carbon: pH and temperature-universal hydrogen release from water reduction. *Energy & Environmental Science* **2018,** *11* (4), 800-806.